ORIGINAL ARTICLE

JBMR®

Role of Fas and Treg Cells in Fracture Healing as Characterized in the Fas-Deficient (lpr) Mouse Model of Lupus†

Maisa O Al-Sebaei,[1,2] Dana M Daukss,[1] Anna C Belkina,[3] Sanjeev Kakar,[1] Nathan A Wigner,[1] Daniel Cusher,[1] Dana Graves,[4] Thomas Einhorn,[1] Elise Morgan,[1,5] and Louis C Gerstenfeld[1,3]

[1]Orthopaedic Research Laboratory, Boston University School of Medicine, Boston, MA, USA
[2]King Abdul Aziz University, Faculty of Dentistry, Department of Oral and Maxillofacial Surgery, Jeddah, Saudi Arabia
[3]Flow Cytometry Core Facility, Boston University School of Medicine, Boston, MA, USA
[4]University of Pennsylvania School of Dental Medicine, Philadelphia, PA, USA
[5]Department of Biomedical Engineering, Boston University School of Engineering, Boston, MA, USA

ABSTRACT

Previous studies showed that loss of tumor necrosis factor α (TNFα) signaling delayed fracture healing by delaying chondrocyte apoptosis and cartilage resorption. Mechanistic studies showed that TNFα induced Fas expression within chondrocytes; however, the degree to which chondrocyte apoptosis is mediated by TNFα alone or dependent on the induction of Fas is unclear. This question was addressed by assessing fracture healing in Fas-deficient B6.MRL/Fas^{lpr}/J mice. Loss of Fas delayed cartilage resorption but also lowered bone fraction in the calluses. The reduced bone fraction was related to elevated rates of coupled bone turnover in the B6.MRL/Fas^{lpr}/J calluses, as evidenced by higher osteoclast numbers and increased osteogenesis. Analysis of the apoptotic marker caspase 3 showed fewer positive chondrocytes and osteoclasts in calluses of B6.MRL/Fas^{lpr}/J mice. To determine if an active autoimmune state contributed to increased bone turnover, the levels of activated T cells and Treg cells were assessed. B6.MRL/Fas^{lpr}/J mice had elevated Treg cells in both spleens and bones of B6.MRL/Fas^{lpr}/J but decreased percentage of activated T cells in bone tissues. Fracture led to ~30% to 60% systemic increase in Treg cells in both wild-type and B6.MRL/Fas^{lpr}/J bone tissues during the period of cartilage formation and resorption but either decreased (wild type) or left unchanged (B6.MRL/Fas^{lpr}/J) the numbers of activated T cells in bone. These results show that an active autoimmune state is inhibited during the period of cartilage resorption and suggest that iTreg cells play a functional role in this process. These data show that loss of Fas activity specifically in chondrocytes prolonged the life span of chondrocytes and that Fas synergized with TNFα signaling to mediate chondrocyte apoptosis. Conversely, loss of Fas systemically led to increased osteoclast numbers during later periods of fracture healing and increased osteogenesis. These findings suggest that retention of viable chondrocytes locally inhibits osteoclast activity or matrix proteolysis during cartilage resorption.

KEY WORDS: CHONDROCYTES; OSTEOCLASTS; FAS; APOPTOSIS; TREG CELLS

Introduction

Studies of the role of TNFα in fracture healing have demonstrated that the expression of TNFα acutely increases during the inflammatory period (within the first 3 days after injury). Subsequently during the initial periods of active cartilage formation, the expression of TNFα and its receptors are almost absent, but then they reemerge as the cartilage undergoes resorption. As resorption proceeds, the key regulatory factors in osteoclastogenesis, receptor activator of NF-κB ligand (RANKL) and osteoprotegerin (OPG) (two other members in the TNF superfamily), as well as macrophage colony-stimulating factor (M-CSF) all become elevated.[1,2] We have also shown that TNF receptor signaling appeared to coordinate aspects of cartilage resorption and primary bone remodeling with angiogenesis.[3] Studies assessing the functional role of TNFα signaling in fracture healing using transgenic mice deficient in TNFRSF1A and TNFRSF1B knockout mice demonstrated that there are three biological processes by which the absence of TNF signaling affects the progression of fracture healing: 1) a delay in the initial healing phase, in either recruitment of mesenchymal cells or the initiation of these cells to undergo skeletogenic cell differentiation; 2) a delay in chondrocyte apoptosis during the period of endochondral bone formation; and 3) a delay in the resorption in the mineralized cartilage during the endochondral period.[2] In summary, a comparison of these various data sets suggests that

Received in original form July 20, 2013; revised form December 10, 2013; accepted December 28, 2013. Accepted manuscript online February 20, 2014.
Address correspondence to: Louis C Gerstenfeld, PhD, Orthopaedic Research Laboratory, Department of Orthopaedic Surgery, Boston University School of Medicine E243, 72 East Concorde Street, Boston, MA 02118, USA. E-mail: lgersten@bu.edu
Additional Supporting Information may be found in the online version of this article.
†The copyright line in this article was changed on August 26, 2014 after original online publication.

Journal of Bone and Mineral Research, Vol. 29, No. 6, June 2014, pp 1478–1491
DOI: 10.1002/jbmr.2169

TNFα signaling plays a crucial role in promoting postnatal bone repair through the recruitment or induction of skeletal cell progenitors,[4,5] carries out a primary role in the regulation of chondrocyte apoptosis,[2,6] and plays a role in regulating the production of factors that control the resorption and vascularization of mineralized cartilage.[3]

In our analysis of the mechanisms by which TNF receptor signaling affected fracture healing, we showed that TNFRs induced the expression of multiple members of the larger TNF family of ligands and TNF receptors, including Fas, TRAIL, VEGI, and OPG.[6] Fas ligand (FasL) is unique among these family members because it binds only to Fas receptor and appears to be primarily involved in mediating apoptosis.[7] Although Fas and FasL play specific functional roles in immune cell differentiation,[8,9] Fas also has been shown to mediate osteoclast apoptosis and loss of estrogen leads to prolongation of an osteoclast's life span, which contributes to sex hormone–dependent osteoporosis.[10,11]

Interestingly, the Fas receptor and its ligand were found to be uniquely expressed during chondrocyte hypertrophy.[12,13] Fas has been found in osteoarthritic cartilage, and treatment of human articular chondrocytes with Fas ligand in vitro causes apoptosis.[14] During development, Fas system has been shown to be present in growth plate chondrocytes in vivo[13,15] which has led to the suggestion that Fas plays a role in chondrocyte apoptosis during endochondral development. We have shown that within the fracture callus, chondrocytes express Fas[2] and that TNFα will induce Fas expression in both repair and articular chondrocytes.[6,13,16,17] Thus, both TNFα and Fas have been implicated in providing death signals to chondrocytes. TNFα promotes apoptosis of both hypertrophic and nonhypertrophic chondrocyte populations through both Fas- and TNFα-mediated signaling, whereas articular chondrocytes undergo apoptosis in response to TNFα.[6,17]

The aforementioned studies on the role of TNFα in fracture healing and in articular cartilage suggested that TNFα facilitates apoptosis of chondrocytes through two distinct processes, a direct induction of apoptosis by TNFα itself and an indirect effect produced by the upregulation of Fas expression.[6,17] Because both TNFRs and Fas can mediate apoptosis and their ligands work in a complex microenvironment in which hematopoietic and mesenchymal cell populations interact with each other, a mechanistic understanding of these two proteins' function will only come from sorting out how TNF and Fas receptors coordinate their activities to keep in balance the progression of apoptosis while promoting skeletal tissue repair after injury. To assess the effects of Fas separate from TNF receptor signaling during fracture healing, we examined fracture healing in B6.MRL/Fas^{lpr}/J mice, which have an inactivating mutation in Fas. These mice develop a generalized lymphoproliferative syndrome and have been used as a model of Systemic Lupus Erythematosus (SLE) because they both produce auto-antibodies and immune-mediated glomerulonephritis.[18–20] Thus, our studies will also present an opportunity to assess how a systemic autoimmune SLE like pathology will effect fracture healing.

Materials and Methods

Mouse strain

All animal research was conducted under an IACUC-approved protocol in conformity with all federal and USDA guidelines. For these studies, we used mice in which the lpr mutation had been bred onto the C57/BL/6 strain (B6.MRL-Fas^{lpr}/J) (Jackson Research Laboratories, Bar Harbor, ME, USA). The choice of strain backgrounds was based on two separate considerations. The first was that a C57/BL/6 background allowed direct comparisons with our previous studies of the TNFRSF1A-/- TNFRSF1B-/- mice.[2] The second consideration was that the lpr mutation in the MRL background manifests a much greater severity of lymphadenopathy[21] with an onset as early as 8 weeks, which could confound our fracture studies. In contrast, the B6.MRL-Fas^{lpr}/J show onset of the lupus-like syndrome after 15 weeks.[22]

Generation of femur fractures

All studies were performed on male 8- to 10-week-old mice. Unilateral midshaft femoral fractures were produced in the left femur as previously described.[23] The location and quality of fractures as well as the position of the intramedullary spinal needle that was used to fix the fracture were assessed while animals were still anesthetized using a standard X-ray machine. (Sirona, Inc., Charlotte, NC, USA). Fractures that were found to be profoundly displaced or comminuted were excluded.

Specimen harvests and sample sizes

Animals were euthanized by CO_2 asphyxiation. Six fractured femora from each strain were harvested on each of days 0, 3, 5, 10, 14, 21, and 28 for RNA extraction and molecular analysis. Three calluses were used to make duplicate pools of mRNAs for analysis. Eight to 11 fractured femora from each strain were collected on days 21 and 35 for micro-computed tomography (CT) and mechanical testing. Five fractured femora from each strain were harvested on days 14 and 21 for histological assessment. Samples for each type of analysis were harvested and prepared as previously described.[23] Five fractured and nonfractured femora from each strain were harvested on days 0 and 10 for flow cytometric analysis.

Quantitative micro-CT

Immediately before scanning, individual femora were removed from storage and allowed to thaw to room temperature. Bones were then prepared for scanning by removal of the intramedullary pins. Scans were preformed using a Scanco μCT 40 system (Scanco Medical, Bruttisellen, Switzerland). Calluses were scanned ex vivo at a resolution of 12 m/voxel. Scanning protocols and initial image-processing methods (reconstruction, noise reduction) were as described previously.[24] The phenotypic properties that were quantified were total callus volume (TV), total mineralized callus volume (BV), mineralized callus volume fraction (BV/TV), average tissue mineral density (TMD), standard deviation of the tissue mineral density ($_{TMD}$), and callus mineral content (BMC). Calculation of TMD, $_{TMD}$, and BMC were made possible by density calibration data obtained from scans of a hydroxyapatite phantom provided by the CT system manufacturer. Based on prior studies, both TMD and $_{TMD}$ were calculated using only the image voxels whose intensity (gray value) exceeded a 45% threshold that distinguishes mineralized tissue from unmineralized and poorly mineralized tissue.[24]

Mechanical testing

After CT scanning, calluses were subjected to biomechanical testing at the specified days as previously described.[24] All specimen preparation and testing was performed blind. Specimens were kept frozen at –20°C until right before they were prepared for torsional testing. Just before testing, the proximal

and distal ends of the bone were potted in polymethylmethacrylate (PMMA). The gage length (exposed length between the potted ends) was measured at 90° intervals around the specimen circumference. Torque (torsional moment) was applied to the specimen, via the aluminum casings, at a rate of 1°/s to failure using a microtorsion testing system (55MT1; Instron Corporation, Canton, MA, USA) equipped with 0.225 N-m torque transducer to measure torque and a high-resolution (0.168 arc-min) internal RVDT to measure angular displacement (twist). Data from both transducers were recorded at a rate of 50 Hz. From the resulting torque-twist curve, the maximum torque, torsional rigidity, and work to failure were calculated.[24]

Demineralized histomorphometry and immunohistochemistry analysis

Tissue retrieval, fixation, demineralization, and sectioning were as previously described.[25] The histomorphometric assessment of osteoclast numbers was based on tartrate-resistant acid phosphatase (TRAP) staining with osteoclast cell counts per mm^2 surface area.[26] Antibody staining was carried out at the Boston University Immuno-histochemistry Core facility using an automated slide stainer (IntelliPATH FLX System, BioCare Medical, Inc., Concord, CA, USA). Antigen retrieval was done with trypsin for 15 minutes, and the slides were blocked with 10% goat serum and Rodent M blocking IgG for 2 hours. For immunohistochemistry, sections were incubated with rabbit polyclonal primary antibodies against Caspase 3 obtained from Cell Signaling Technology Inc. (Danvers, MA, USA) at 1:200 dilution for 2 hours at 4°C. Secondary reactions were carried out using Alexa Fluor 488 Goat Anti-Rabbit IgG (H + L) from Invitrogen Inc. (Carlsbad, CA, USA) at a dilution of 1:500, and reactions were for 1 hour at room temperature. DAPI was obtained as ProLong Gold reagent liquid mountant from Invitrogen Inc. Slides were then washed in TBST for 2 minutes. All photomicrograph images were taken and collected on an Olympus Microscopy System (Olympus America Inc., 3500 Corporate Pkwy, Center Valley, PA, USA) using a Blue (DAPI): Chroma 31000v2 Green (Immunofluorescense): Chroma 41028 Red (TRAP): Chroma 49005 filter.

Messenger RNA analysis

Total RNA samples were assessed in a duplicate set of pooled samples prepared from three to four fractured calluses harvested on 3, 5, 10, 14, 21, and 28 days after fracture. Reference RNA was prepared from a duplicate set of pooled samples prepared from three to four 5-mm segments of unfractured mid-diaphyseal femurs. Total RNA was extracted and purified as described by Wang and colleagues.[27] The two pools of mRNA samples were then used for each mRNA analysis, which was carried out three times for each pool of RNA. Ribonuclease protection assays (RPA) were carried out as described by Cho and colleagues,[28] using 3 μg to 10 μg of total mRNA dependent on the template set. All template sets included GAPDH and L32 probes as internal standards. RNA samples were compared via autoradiographic analysis and normalized to the L32 housekeeping gene to ensure that the samples were intact and uniformly loaded. All reagents for the qRT-PCR analysis were from Applied Biosystems, Inc. (Foster City, CA, USA), and plate assays were read on an ABI 7700 Sequence Detector (Applied Biosystems). A summary of probe information for each primer is provided in Supplemental Table S1. Two micrograms of total RNA was used for each preparation of cDNA. All cDNA preparations were generated by random hexamer priming. Reverse transcription reactions and PCR conditions were as previously reported.[27] The18S rRNA was used for normalization of each target sequence. Each pooled RNA sample was run 3 times. The fractional cycle number at which the fluorescence passes the fixed threshold (C^T values) was used for quantification by using a comparative C^T method. Mean expression values were determined from the six measurements.

FACS analysis

For phenotypic analysis of the T- and B-cell complements, spleens, femora, and callus tissues were isolated from 10-week-old wild-type B6 and B6.MRL/Fas^{lpr}/J mice for baseline measurements (before fracture) and 10 days after fracture ($n = 5$ mice per group). Femora and adjacent callus tissues were crushed to liberate cells into DMEM medium supplemented with 10% fetal bovine serum, penicillin, and streptomycin. Bone fragments were removed by sterile filtration with 70-μm strainers (BD Biosciences, San Jose, CA, USA). Splenocytes were prepared by mechanical disruption of the spleens. For all samples, erythrocytes were removed with red blood cell lysis buffer (BioLegend, San Diego, CA, USA), and resulting cell pellets were resuspended in FACS staining buffer (eBioscience, San Diego, CA, USA). Cells were stained with the following monoclonal antibodies in presence of Fc Block (eBioscience): CD4 FITC and CD25 PE (Mouse Regulatory T Cell Staining Kit, eBioscience), CD19 APC-Cy7, CD3 PerCP, and CD69 Pacific Blue (BioLegend). For intracellular staining with anti-Foxp3 APC antibodies, the cells were first washed, fixed, and permeabilized according to the manufacturer's protocol. Dead cells were excluded based on the staining with Zombie Aqua fixable dye (BioLegend). Data were acquired on BD LSR II SORP (BD Biosciences). At least 100,000 single-cell events were acquired and analyzed with FlowJo 10.0.6 (TreeStar, Ashland, OR, USA) for all samples. Gating determinations were performed with the use of FMO (Fluorescence Minus One) and isotype controls (Supplemental Fig. S1).

Statistical analysis

The data for both the control and experimental groups were presented as means ± standard deviation. The difference between the two groups at each time point was evaluated by Student's *t* test, at a level of significance of $p < 0.05$ for the RNA and histological analysis. For the micro-CT assessments, the effect of time and strain and their interaction was established using two-factor ANOVAs. For the results of the torsion tests, three-factor ANOVAs with time, strain, condition (fractured or unfractured femur), and the interaction between these effects were performed. For the results of FACs analysis, three-factor ANOVAs with time, strain, condition (fractured or unfractured femur), and the interaction between these effects were performed. When applicable, a Tukey post hoc test was used to identify pairwise differences. A significance level of $p = 0.05$ was used in all cases.

Results

Quantitative micro-CT

Representative three-dimensional reconstructions of longitudinal half-sections of the fracture callus are presented in Fig. 1. The most striking feature of these comparisons was the increased porosity in the bony calluses from the B6.MRL-Fas^{lpr}/J mice. Quantitative measurements of the structural and mineral compositions of the calluses' tissues are presented in Fig. 1*B*. Both the total volume of the callus and the volume of mineralized

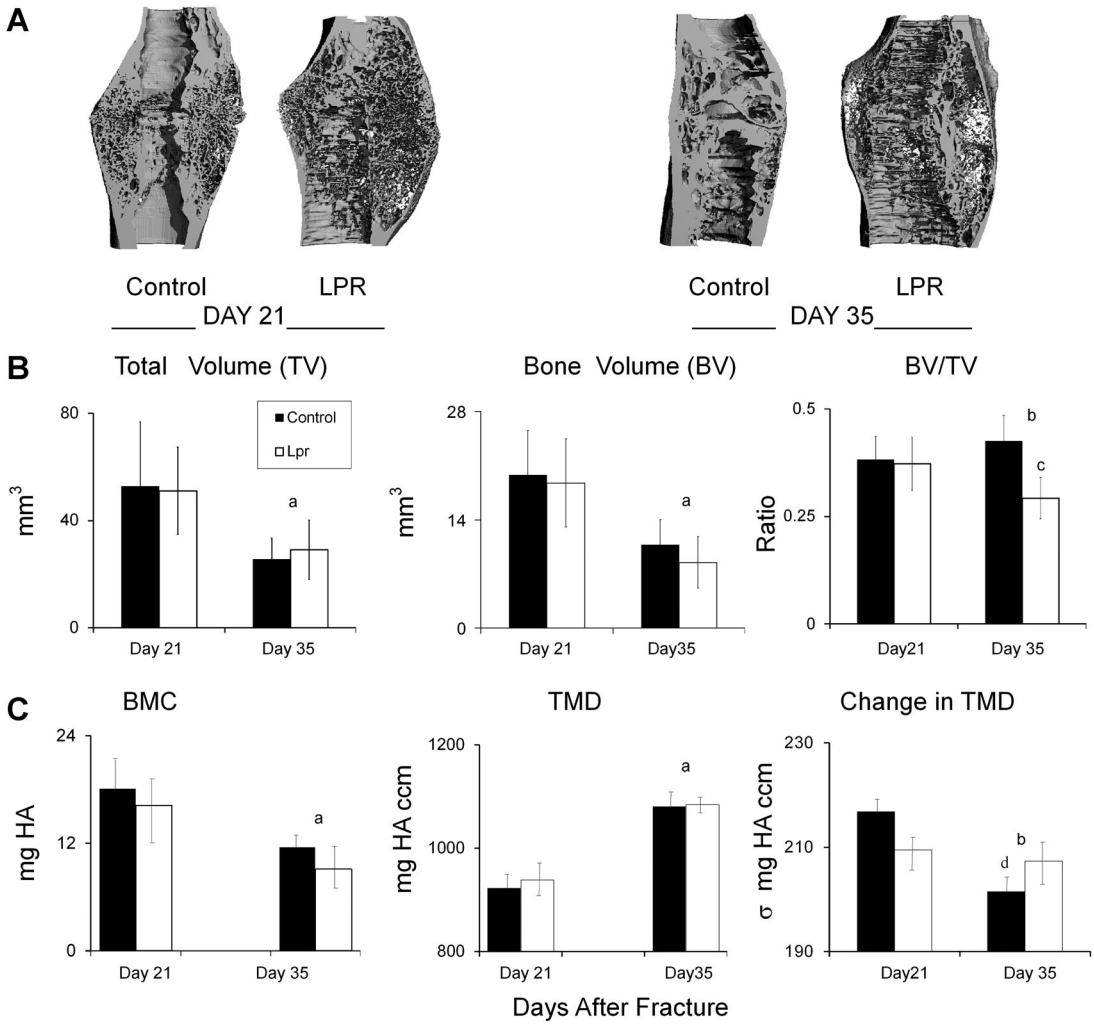

Fig. 1. Callus microstructure at 21 and 35 days after fracture as assessed by micro-CT. (*A*) Representative renderings on days 21 and 35 days after fracture. The reconstructed images were cut longitudinally to show the internal microstructure. (*B*) Graphical analysis of the structural micro-CT measurements of fracture calluses at 21 and 35 days after fracture. (*C*) Graphs showing characteristics of differences based on mineral content. The error bar is ± SD. a = significance by time; b = significant interaction by time and strain; c = difference by strain at a single time point; d = difference by time for a single strain. Significance was at $p < 0.05$.

tissue in the callus were smaller in the day 35 time point compared with the day 21 day time point and did not differ between strains ($p < 0.0001$). On the other hand, the overall ratio of volume of mineralized tissue to total callus volume was lower in the B6.MRL-Fas^{lpr}/J mice than in the controls at day 35 ($p = 0.007$). The tissue mineral density of the callus increased over time, whereas the total mineral content decreased over time in both strains ($p \leq 0.0005$). The standard deviation of the tissue mineral density decreased over time only in the control mice ($p = 0.0161$). Identical findings were observed in the *gld* mouse strain in which Fas has been completely deleted in contrast to the lpr strain in which it is functionally defective (Supplemental Fig. S2).

Mechanical testing

Results of the torsion tests are summarized in Fig. 2. The fractured control femora withstood a higher maximum torque than the B6.MRL-Fas^{lpr}/J strain ($p = 0.0051$) (Fig. 2). None of the other torsional properties differed between strains, between time points, or between fractured versus contralateral bones, although the fractured bones always showed statically ($p = 0.05$) less torsional strength than the unfractured contralateral femora. The latter result suggested that by 21 days these other properties have all been regained in the fractured bones.

Histomorphometric analysis

Callus tissues at 14 and 21 days after fracture were examined because these time points are representative of key transitional points in the resorption of the mineralized cartilage (day 14) and the maximal period of primary bone formation (day 21). Qualitatively, the B6.MRL-Fas^{lpr}/J calluses looked larger and had more cartilage tissues present at 14 days after facture with small remnants of cartilage tissue still observed at 21 days after

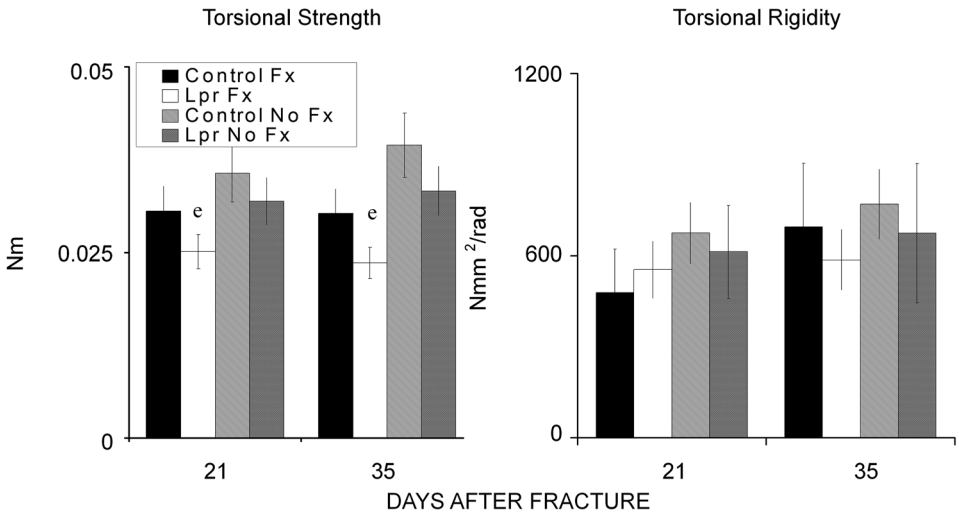

Fig. 2. Results of the torsion tests. (Left panel) Comparison of torsional strength (in Nm) of the calluses from control and B6.MRL-Fas^{lpr}/J mice at 21 and 35 days after fracture and of contralateral femora from the two genotypes at matching time points. (Right panel) Comparison of torsional rigidity (in Nmm^2/rad) among these same groups. e = significance by strain. The error bar is ± SD. Significance was at $p < 0.05$.

fracture compared with the control specimens (Fig. 3*A*). Higher magnification of regions of trabecular tissues at 21 days after fracture provided corroborating data to the micro-CT findings, showing that there was less trabecular tissue at this time (Fig. 3*B*). Quantitative measures of the total callus cross-sectional areas for both control and B6.MRL-Fas^{lpr}/J strain were higher in day 14 after fracture calluses ($p < 0.0001$) than day 21 calluses, whereas calluses from the B6.MRL-Fas^{lpr}/J strain had a greater area than the control calluses at both time points ($p < 0.0001$). The measured area of bone in the calluses did not change between days 14 and 21; however, it was significantly less in the B6.MRL-Fas^{lpr}/J strain regardless of the time point ($p < 0.0013$). In contrast, the amount of cartilage tissue was greater in the B6.MRL-Fas^{lpr}/J strain (Fig. 3*C*) at both time points. Separate assessments based on the percentages of tissue compositions are presented in Table 1, and a summary of the statistical analysis of interaction between time and strain for each of the separate measurements is presented in this table.

Analysis of cartilage and bone cell mRNA expression

Molecular assessments of mRNA expression for a number of families of different genes were carried out to further determine how the *lpr* mutation led to the changes in tissue compositions that were seen in the fracture specimens. The mRNA expression that encodes a group of extracellular matrix proteins, which would be indicative of both cartilage and bone development and differentiation, were assessed by RPA. A representative autoradiograph of an RPA of selected extracellular matrix protein mRNAs across the time course of fracture healing is seen in Fig. 4. The graphic results for four of the expressed mRNAs that were examined by the RPA are shown at the bottom of the figure. The expression of all four bone-associated mRNAs (type I collagen, osteocalcin, bone sialoprotein, and osteopontin) all showed increased expression in B6.MRL-Fas^{lpr}/J mice, with all of them having statistically higher levels of expression at 21 and 28 days after fracture ($p = 0.045$). Intermediate- and early-late-stage markers of osteogenesis as determined by expression of osteopontin and BSP also showed both an early (day 3) and later peaks in expression (day 14) and also showed higher levels of expression in the B6.MRL-Fas^{lpr}/J on days 21 and 28. Chondrogenesis was assessed by examining the expression of collagen type II (Col2A1) and collagen type X (Col10A1). Both of these mRNAs peaked at day 10 in the control calluses, whereas the Col10A1 peak was broader and lagged that of Col2A1 in the B6.MRL-Fas^{lpr}/J calluses.

Assessment of tissue resorption and remodeling

Osteoclast numbers in the calluses were next examined as a measure of tissue resorption and remodeling. Low-magnification images of the total cross-sectional areas of the callus provide a global qualitative assessment of number of osteoclasts within the tissue (Fig. 5*A*, upper panels). Although callus tissues from both the control and B6.MRL-Fas^{lpr}/J strain had observable amounts of TRAP-positive cells, the B6.MRL-Fas^{lpr}/J strain appeared to show more activity. Higher magnifications showed individual TRAP-positive multinucleated cells both on surfaces of new primary bone as well as on the surfaces of mineralized cartilage (Fig. 5*B*). Consistent with our previous studies, the greatest number of osteoclasts were seen during the period of resorption of the mineralized cartilage (day 14) and decreased with time ($p < 0.0001$), and this interaction between time and strain was significant ($p < 0.0024$). The Tukey post hoc test showed that the day 14 B6.MRL-Fas^{lpr}/J strain had a higher osteoclast count than any of the other specimens that had been analyzed (Fig. 5*C*). An overall summary of all of the histomorphometric measurements and indices and their statistical significance is presented in Table 1.

A selected set of markers associated with the regulation and progression of osteoclast differentiation were measured (Fig. 5*D*). The ratio of RANKL to OPG was determined because this ratio is the central factor that controls osteoclastogenesis.

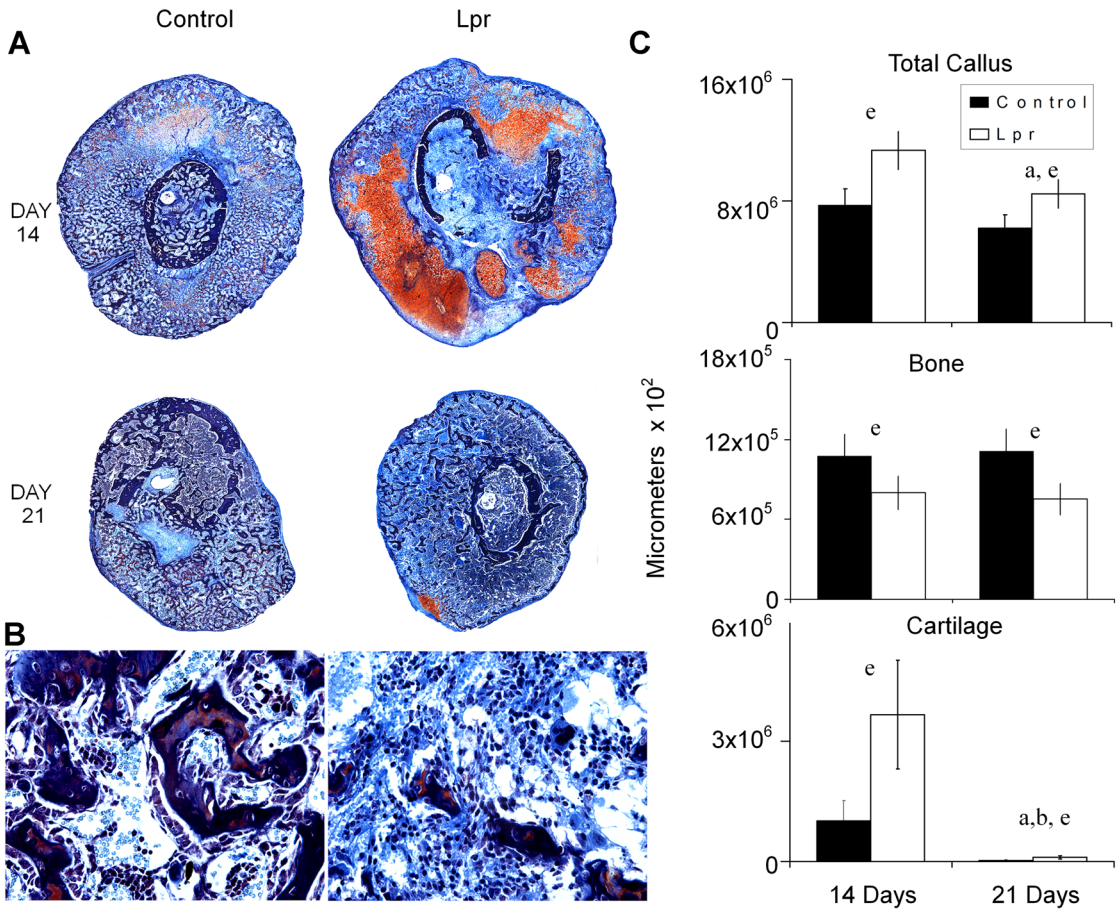

Fig. 3. Histological analysis of fracture calluses at days 14 and 21 days after fracture (safranin-O and fast green). (*A*) Representative micrographs from 14 and 21 days after fracture. (Top panel) Composite images of fracture calluses (×100 magnification). (*B*) Representative micrographs of trabecular and medullary tissues at 21 days after fracture (×200 magnification). (*C*) Graphic analysis showing the total callus area, total cartilage area, and total bone areas in μm^2 as calculated from the histomorphometric analysis for the control and B6.MRL-Fas^{lpr}/J strains at days 14 and 21 days after fracture. The mean value from 5 representative sections per callus (a total of 5 calluses were used per time point) are shown. The error bar is ± SD. Group differences are as denoted in Fig. 1. Statistical comparisons between strains times and interactions are as denoted by letters and are as presented in Figure legends 1 and 2. Significance was at $p < 0.05$.

During the initial periods of endochondral bone formation, there was no difference for the mRNA expression ratio in the two strains, but by day 10 the B6.MRL-Fas^{lpr}/J showed a higher ratio than observed in the controls and this higher ratio then persisted throughout the period of coupled remodeling of primary bone at 21 and 28 days after fracture. An assessment of M-CSF, the other major regulator of osteoclast development, showed a more prolonged period of later expression slightly preceding and then paralleling the higher RANKL/OPG ratio. The fold change in both TRAP and calcitonin receptor expression for both strains sharply increased at day 10, after which the levels of expression remained elevated until day 21, when they began to return to its baseline. Although TRAP expression levels were greater at 14 days in the B6.MRL-Fas^{lpr}/J than the control, this difference was not significant. On the other hand, calcitonin receptor expression peaked earlier and was lower in the control samples and was statistically higher at both 21 and 28 days after fracture in the B6.MRL-Fas^{lpr}/J strain ($p < 0.05$). It is interesting to note that because calcitonin receptor expression is associated with fully mature osteoclasts, its more prolonged levels of expression would be suggestive that these cells have a longer life span in the B6.MRL-Fas^{lpr}/J strain.

Assessment of the inflammatory state and T-cell activity during endochondral bone formation

To assess if the autoimmune phenotype of the B6.MRL-Fas^{lpr}/J strain affected endochondral bone formation or bone turnover during fracture healing, several different pro- and anti-inflammatory cytokines that have been shown to have altered expression during an active autoimmune state were assessed (Fig. 6*A*). As expected, these data showed that the expression of TNF-α, IL-1β, and IL-17F all were constitutively higher in the B6.MRL-Fas^{lpr}/J. In contrast, cytokines that would prevent the T cells from progressing to a Th1 phenotype (IL-10, IL-17A) were elevated in the mutant mice, whereas those that have been shown to inhibit Th17 development toward an iTreg (IL-6 IL-23) also showed diminished initial induction after fracture in the B6.MRL-Fas^{lpr}/J mice.[29] Using CD4 as a general assessment of T cell numbers also showed lower levels of CD4 mRNA initially after fracture in the wild-type mice. A comparison of

Table 1. Mean Values for the Histomorphometric Measurements and Indices

Measurement or index	Control Day 14	Lpr Day 14	Control Day 21	Lpr Day 21
Total callus area (mm^2)				
Mean	8.68	12.7	6.98	9.51
SD	3.45	2.87	3.07	2.62
Time	$p < 0.00001^*$			
Strain	$p < 0.0001^*$			
Time × strain	$p = 0.2040$			
Percentage of bone per callus				
Mean	0.123	0.062	0.236	0.076
SD	0.071	0.0052	0.0403	0.0058
Time	0.1292			
Strain	0.0096^*			
Time × strain	0.2389			
Percentage of cartilage per callus				
Mean	0.065	0.224	0.002	0.007
SD	0.011	0.011	0.0006	0.001
Time	$p < 0.0001^*$			
Strain	$p < 0.0001^*$			
Time × Strain	$p < 0.0001^*$			

The p values are shown for two-way ANOVA with the effects of time, strain, and the interaction of time and strain.

*Statistical significance at $p < 0.05$.

SD = standard deviation; Control = C57BL/B6; lpr = B6.MRL/Fas^{lpr}/J.

these cytokine patterns across the time course of fracture healing further showed that there was reciprocal down-regulation and upregulation of the cytokines that drive Th1 and iTreg differentiation, respectively, during the period of cartilage formation in both B6.MRL-Fas^{lpr}/J and wild-type callus tissues.

As a second assessment of the autoimmune state, FACS analysis was performed to determine the T-cell subset distribution in the spleen and femora at both the baseline before fracture and at 10 days after fracture. At the later time point, contralateral femora were further compared with the callus tissues of the fractured bones. These results revealed that B6.MRL-Fas^{lpr}/J mice had higher levels of Treg cells within both the bone and spleen at baseline before fracture (Fig. 6*B*, *C*). In both wild-type mice and B6.MRL-Fas^{lpr}/J mice, fracture appeared to systemically increase Treg percentages, ~60% and ~30%, respectively, within both the fractured and contralateral femur (Fig. 6*B*) while having no effect on the numbers of these cells in the spleen (Fig. 6*C*, Supplemental Fig. S1). The percentage of activated T cells in the bone at the baseline was less in B6.MRL-Fas^{lpr}/J mice than in wild-type mice. After fracture, the Treg levels decreased in the callus tissues of the wild-type mice within the callus tissues while remaining unchanged in the B6.MRL-Fas^{lpr}/J mice. Unlike Treg cells that showed systemic changes in the contralateral bones, the percentage of activated T cells, as determined by CD69 expression, remained unchanged for both wild-type and B6.MRL-Fas^{lpr}/J mice within the unfractured femur. Further, within the spleen, the percentage of activated T cells was always higher in the B6.MRL-Fas^{lpr}/J mice both at the baseline and at 10 days after facture, and these levels are unchanged in response to fracture. Analysis of the percentage B cells in bone tissues showed no changes either between strains of mice or in response to fracture. In contrast, the percentage of these cells in the spleen was less in the B6.MRL-Fas^{lpr}/J mice at both the baseline and after fracture (data not shown).

Assessment of tissue apoptosis

In the last analysis that is presented, a qualitative assessment of the number of cells that were primed to undergo apoptosis was carried out using immunohistological staining for the expression of caspase 3. We examined the callus tissues at 14 days after fracture because both cartilage tissue and high levels of osteoclasts were observed at this time (Fig. 7). An examination of comparable areas of cartilage tissue in the B6.MRL-Fas^{lpr}/J and wild-type mice showed that there were many more chondrocytes showing strong green fluorescent-staining cells for the presence of the capsase 3 in the wild-type callus tissues than in the B6.MRL-Fas^{lpr}/J tissues. These images are depicted in the upper panels of the figure. We next carried out sequential reactions first for TRAP and then with caspase 3. Those osteoclasts that showed colocalization with caspase 3 stain orange and are those osteoclasts that would be primed to underage apoptosis. Like the chondrocytes, many more positive osteoclasts were seen in the control samples. These images are depicted in the lower panels of Fig. 7.

Discussion

Both similar and different features in the progression of fracture healing were observed in mice deficient in Fas (B6.MRL-Fas^{lpr}/J) in comparison to mice lacking TNFR signaling. Unlike fracture healing in the absence of TNFR signaling, no delays in the initiation of chondrogenesis was observed. These conclusions are based on two findings: 1) there was no change in the temporal expression of both chondrogenic and osteogenic mRNA expression levels found in the callus tissues of B6.MRL-Fas^{lpr}/J mice at the earliest times points, suggestive that stem cell recruitment was normal during the initial periods of fracture healing; and 2) the callus tissues at day 14 in the B6.MRL-Fas^{lpr}/J mice were larger, which suggests that the formation of the initial tissue analogue was unaffected by this type of systemic

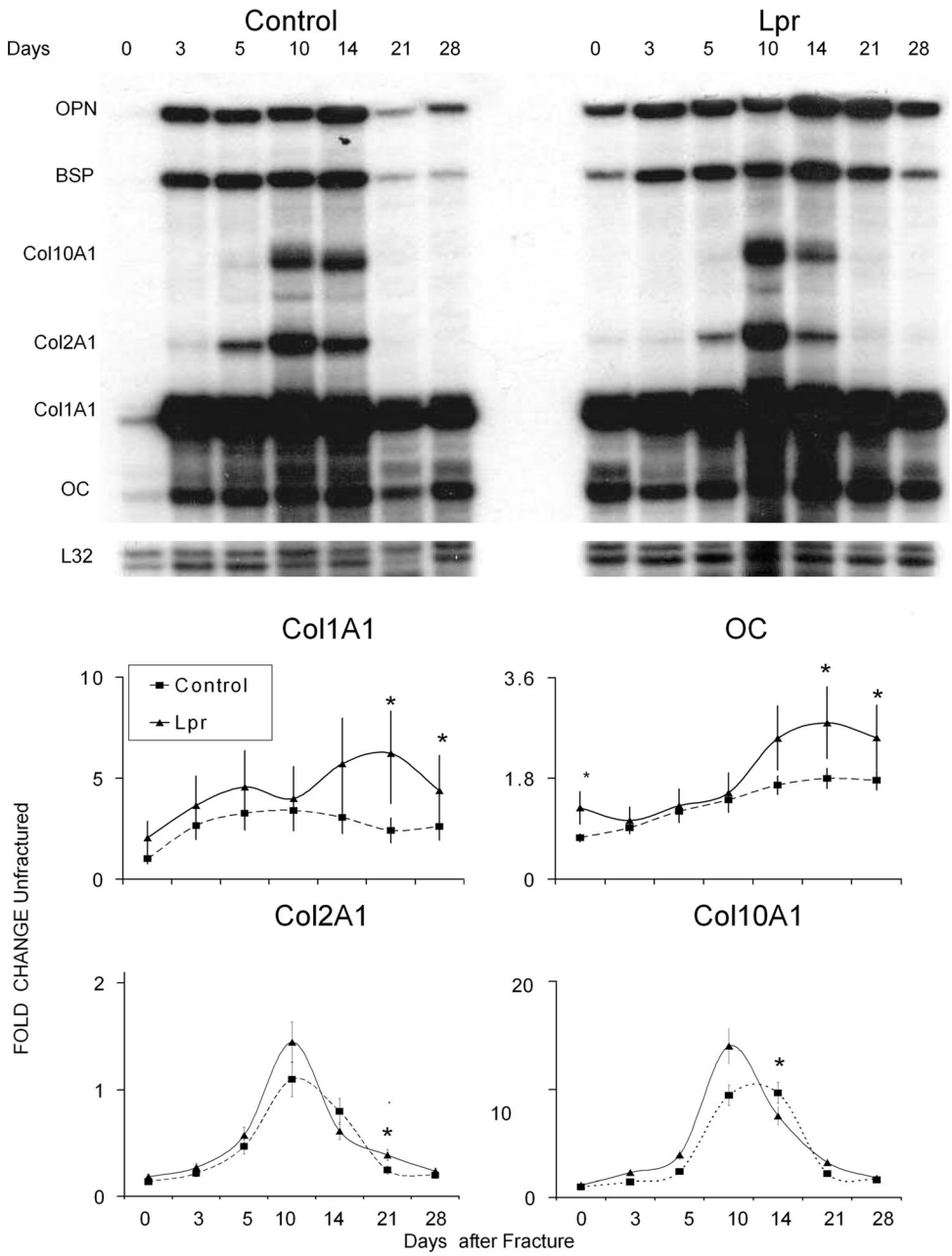

Fig. 4. Analysis of expression of bone- and cartilage-specific mRNAs. (*A*) Representative autoradiographic image of the RPA products as resolved on a 6% denaturing sequencing gel. Matrix genes are depicted. Days after fracture, mouse strain, and positions of each protected gene are denoted in the figure. L32 (mouse ribosomal protein) was used as an internal standard. (*B*) Graphic analysis of the relative mRNA expression levels of four of the mRNAs indicative of either cartilage or bone tissue development obtained from RPA analysis over the time course of fracture healing. The nature of each of the mRNAs that is presented is indicated in the legend of the figure. Data presented are mean values from $n = 4$ gels, and error bars are + SD. *Significance between the two strains at $p < 0.05$.

autoimmune disease. Thus, these results also lend credence to the hypothesis that part of the biological functions of TNFR signaling during early tissue repair is to facilitate early stem cell recruitment, consistent with other results that show that very low doses of locally applied TNFα promote fracture healing.[5]

Although the loss of functional Fas signaling does not appear to effect early callus development, distinct differences in the progression of fracture healing were observed during the periods of cartilage resorption and the remodeling of the primary bone. These results are similar to fracture healing in the TNFR-deficient mice, which also show delayed progression through the endochondral bone formation period, in that higher percentages of cartilage tissues are found in the calluses of the B6.MRL-Fas^{lpr}/J mouse strain through the 21-day-after-fracture period relative to the controls. As described above, because neither the time course nor the amounts of the cartilage mRNA

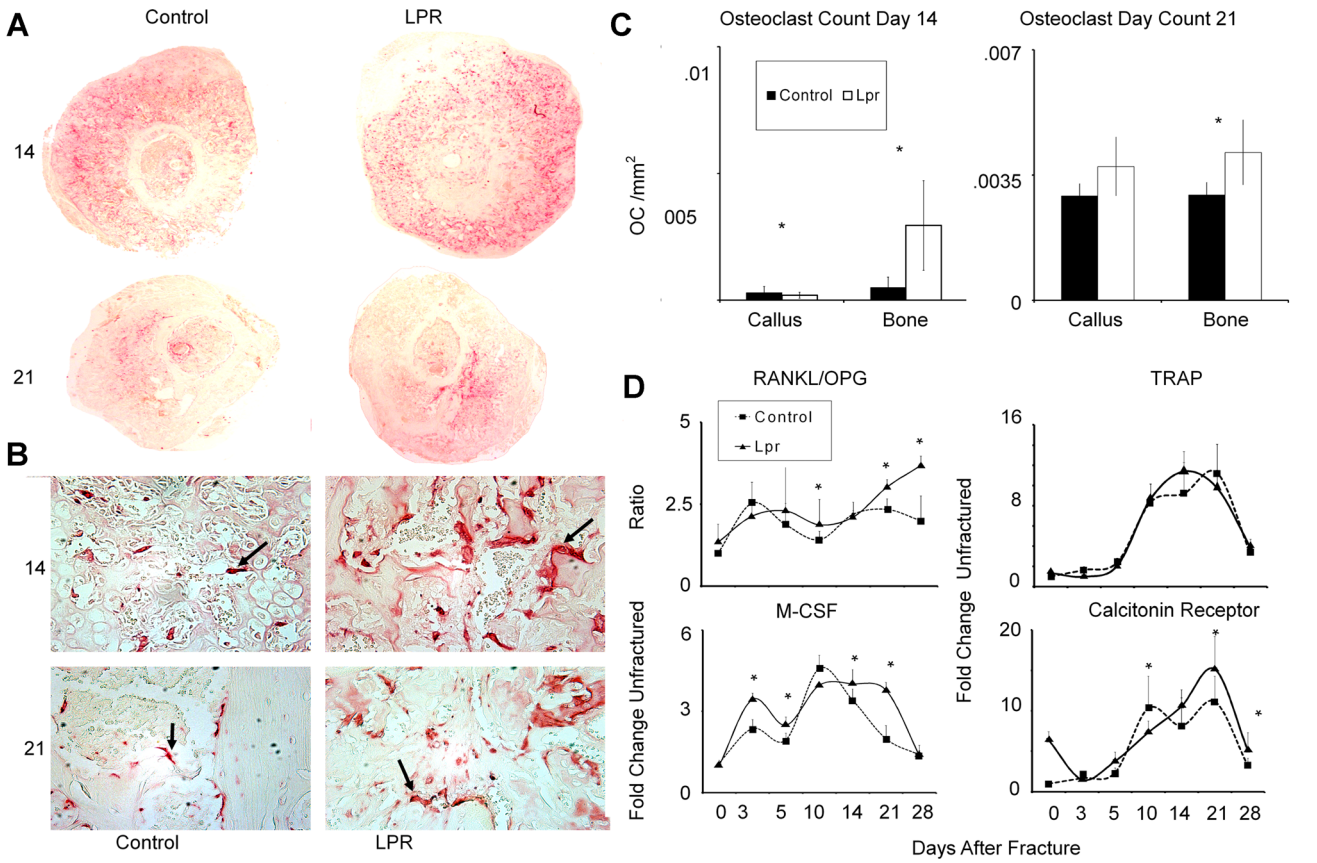

Fig. 5. Analysis of osteoclast activity in fracture calluses. (*A*) Panoramic histological assessments of local osteoclast activity within callus tissues based on TRAP 5b staining within 14- and 21-day callus tissues. Composite images of fracture calluses (×40 magnification). (*B*) Osteoclast morphology on bone/cartilage surface for each strain of mouse (×400 magnification). (*C*) Osteoclast counts per unit total callus area. Osteoclast counts were determined as described in Materials and Methods. Numbers are presented per average area of entire callus and per area of bone surface. (*D*) Analysis of the expression of osteoclast and proresorptive cytokine mRNAs. Graphical representation of the temporal patterns and relative levels of mRNA expression for various mRNAs associated with osteoclasts and the regulation of their expression. mRNA expression levels were determined by qRT-PCR. Days after fracture is denoted, and strain of mice is the same as denoted in the legend in Fig. 4. The nature of each mRNA that is assessed is indicated in the figure. The overall expression of RANKL and OPG are not presented, rather the ratio of the expression of these mRNAs. Data presented are mean values from $n = 6$ replicates determined from two pools of mRNAs per time point. The error bars are + SD. *Significance between the two strains at $p < 0.05$.

expression were initially different, the greater accumulation in cartilage tissues was not the result of greater levels of cartilage development. The statistically higher levels of type X collagen mRNA expression at day 14 after fracture also suggest that the chondrocyte remained in a viable hypertrophic state for a longer period. These results are similar to our previous finding for mice lacking TNFR signaling that showed that increased cartilage contents were the result of delayed cartilage resorption. Such results are consistent with the results that showed a smaller number of chondrocyets stained for caspase 3, which correlates with the suggestion that loss of Fas leads to delayed cartilage apoptosis. Although loss of Fas signaling delayed cartilage resorption, these tissues were eventually removed, suggesting that Fas independently acts in parallel with TNFα to mediate apoptosis, which would be consistent with the persistent higher levels of TNFα expression found in the B6.MRL-Fas^{lpr}/J mouse strain. Alternatively, both these extrinsic death receptors may be working in tandem with other intrinsic mechanisms that mediate chondrocyte apoptosis. In this regard, it is of interest to note that chondrocyte apoptosis during hypertrophic development also appears to be mediated by activation of intrinsic mitochondria mechanisms[30] in which mitochondrial DNA damage and intrinsic activation of apoptosis is caused by pro-inflammatory cytokines in human OA chondrocytes.[31]

In contrast to the delayed resorption of the cartilage tissues within the callus, both histological and micro-CT analysis of the callus tissues at later times showed statistically decreased amounts of accumulated mineralized bone tissues. The assessment of the biological mechanisms that mediated the diminished accumulation of bone showed that this was attributable to increased bone turnover. This conclusion was based both on the significantly higher numbers of TRAP-positive multinucleated cells that lined the bone and mineralized cartilage surfaces in B6.MRL-Fas^{lpr}/J fracture calluses and the greater levels of expressed osteoclast mRNAs. Because the measured area of bone was lower in the B6.MRL-Fas^{lpr}/J strain, the amount of osteoclasts per area of bone and cartilage was even more exaggerated in B6.MRL-Fas^{lpr}/J than control calluses. These results suggest that optimal mineralized cartilage resorption must either be linked to chondrocyte apoptosis or be inhibited by viable chondrocytes.

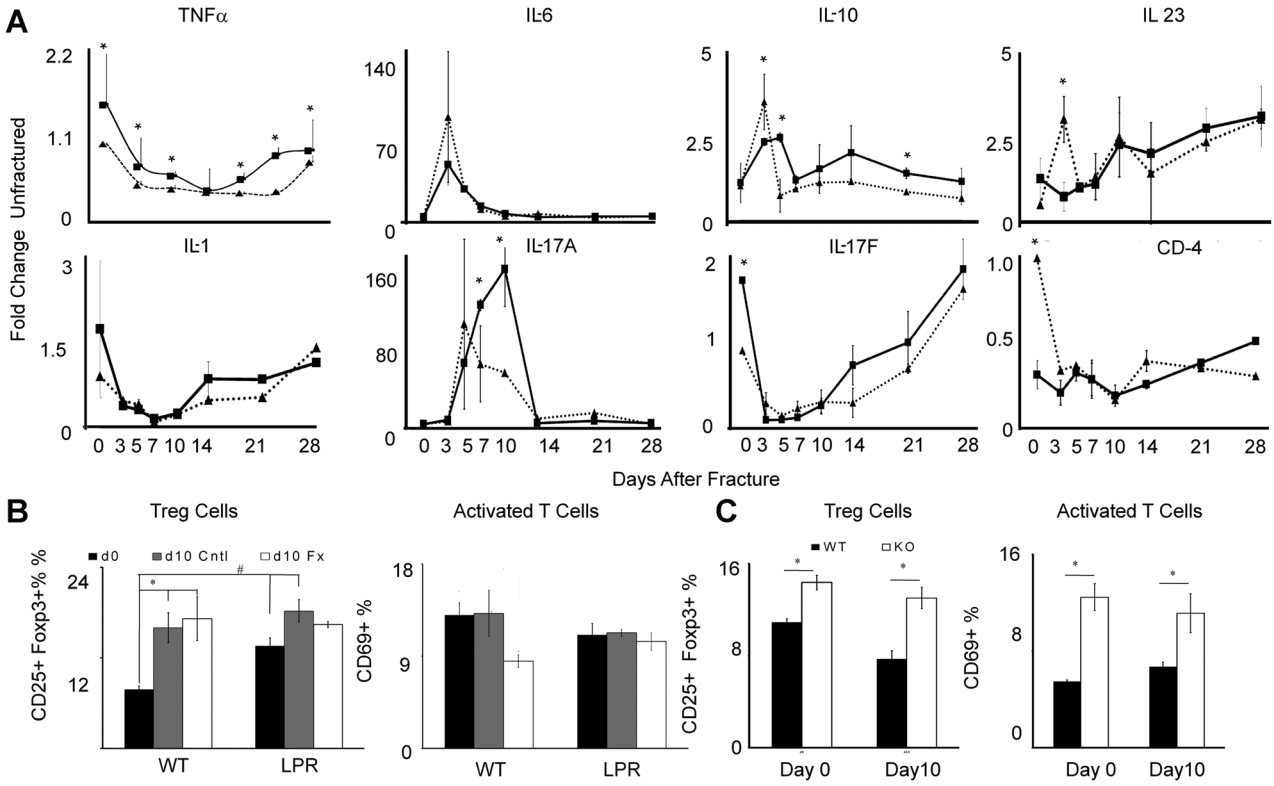

Fig. 6. Assessments of inflammatory state and T-cell activity. (*A*) Graphical representation of the expression of the temporal patterns and relative levels of mRNA expression of select pro- inflammatory and T-cell regulatory cytokines as determined by qRT-PCR. Days after fracture are denoted, and strain of mice is the same as denoted in Fig. 4. The nature of each mRNA that is assessed is indicated in the figure. Data presented are mean values from $n = 6$ replicates determined from two pools of mRNAs per time point. The error bars are + SD of the 6 replicates from the two pools. *Significance between the two strains for that time point $p < 0.05$ based on the comparisons of the replicates. (*B*) Flow cytometric analysis of Tregs and activated T cells in femoral bones at baseline before fracture and in both the contralateral (Cntl) unfractured and fracture (Fx) bone at 10 days after fracture. Tregs were identified as the percentage of CD25 + Foxp3+ of all live CD3 + CD4+ cells, and activated T cells were percentage CD69+ of all CD3 + CD4+ cells. Intragroup: *difference ($p < 0.05$) at day 0 and after-fracture day 10 in either WT or LPR strains. Intergroup: #difference in mice between WT and LPR strains. (*C*) Flow cytometric analysis of Tregs and activated T cells in spleens at baseline before fracture and at 10 days after fracture in both WT and LPR strains. Gating strategy and labeling are the same as in (*B*). A complete summary of the findings for the ANOVA statistical analysis of these data is presented in Supplemental Tables S3–S5.

This conclusion is consistent with recent findings that show that cartilage destruction in polychondritis is induced not only by perichondral inflammation but also by the expression of proteolytic enzymes by the chondrocytes themselves in association with the induction of apoptosis.[32] Our results would also be consistent with this finding and further suggest that proteolytic completion of the mineralized cartilage resorption takes place only when the chondrocytes undergo their apoptosis. In addition, these results suggest that mineralized cartilage resorption must be only partially mediated by osteoclasts given that these cells show no delay in their recruitment in the B6.MRL-Fas^{lpr}/J fracture calluses and are actually present in greater numbers in the mutant mouse tissues.

The comparison of the control and B6.MRL-Fas^{lpr}/J mice fracture suggests that the remodeling phases in which primary bone was being replaced were greatly elevated. This conclusion was based both on multiple findings, including the histological analysis of the trabecular bone parameters in B6.MRL-Fas^{lpr}/J calluses, which had fewer trabeculae that were thinner with an overall greater spacing (more porous); the diminished biomechanical competency of the B6.MRL-Fas^{lpr}/J calluses at 35 days after fracture; and the elevated numbers of TRAP-positive multinucleated cells that were found at later times in the callus tissues. It is interesting to note that the increased numbers of TRAP-positive cells were accompanied by a consistently elevated level of mRNA expression for all of the osteoblast markers that we assayed, including those for both early (Col1a1, OPN) and later (BSP, OC) marker genes for osteoblast differentiation. There was no evidence, though, of increased osteoid production, suggesting that either the osteogenic cells are expressing higher levels of their gene products or that these cells are rapidly turning over and do not form substantial amounts of new osteoid. This later conclusion is consistent with recent studies that have shown that most osteoblast cells are relatively short lived and that they arise from an actively mitotic stem cell/progenitor pool.[33]

Separate mechanisms effecting both initial osteoclastogenesis and prolongation of osteoclast activity and life span may be evoked for the greater numbers of osteoclasts, which were observed in the B6.MRL-Fas^{lpr}/J mouse. Data consistent with

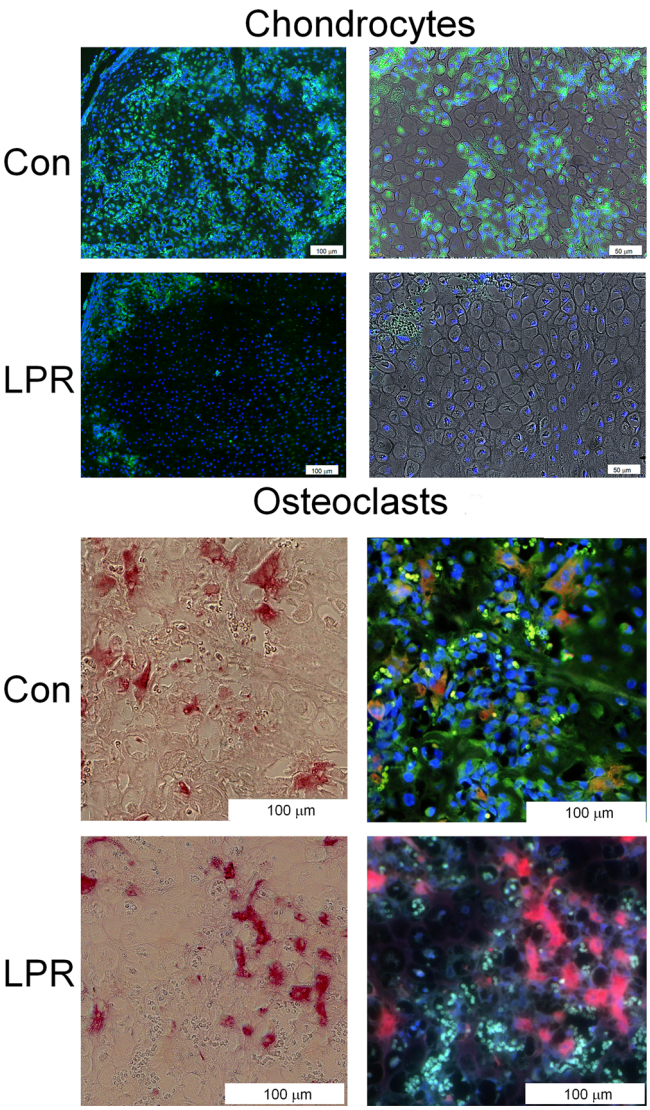

Fig. 7. Immunohistological analyses of chondrocyte and osteoclasts within 14-day callus tissues that show caspase 3 reactivity. Under fluorescent excitation, caspase antibody staining is bright green and red blood cells are autofluorescent and appear as small bright green cells, whereas backgrounds appear as defuse light green. DAPI staining is bright blue and stains the nuclei of cells. Under fluorescent excitation, TRAP staining is red and double-stained cells with caspase stain orange. Under light field, TRAP cells appear as pink-red cells. (Upper panels) Sequential set of micrographs showing fluorescent images of chondrocytes that are reactive with anti-caspase 3 antibody in control (CON) and Lpr strain of mice (LPR). A low-magnification fluorescent image and higher-magnification image from the same field superimposing the fluorescent on light level photomicrograph are presented. Cells were co-reacted with DAPI to identify the nuclei of the individual cells in the micrographs. (Lower panels) Sequential set of micrographs showing light level and fluorescent images of TRAP-positive osteoclasts. Those cells that are reactive with anti-caspase 3 antibody are stained orange, and borders of these cells show a green edge. Cells were co-stained with DAPI to identify the individual cells in the micrographs. Magnification is indicated in each image.

greater levels of initial osteoclastogenesis are related to both the earlier and higher levels of TRAP mRNA expression that were observed in the callus tissues for the B6.MRL-Fas^{lpr}/J mouse. It is interesting to note as well the consistent and statistically higher levels of TNFα mRNA expression and RANKL to OPG ratios that were observed in mutant mice. Mechanistic studies have shown that TNFα is a proresorption cytokine that leads to bone destruction,[34] with some studies showing TNFα inducing bone resorption via its indirect stimulation of both RANKL and M-CSF with commensurate downregulation in OPG expression.[35–37] Other mechanisms have shown that pathologically high TNFα levels lead to direct induction of osteoclastogenesis at the level of blood osteoclast precursors (OCP),[38] whereas other studies have shown that high levels of TNFα directly increases TRAP-positive cells in vitro.[39,40] In context of the mouse *lpr* mutation, it is interesting to note that loss of Fas antigen receptor leads to the development of toxic shock syndrome much faster than in normal mice,[41] with increased expression of TNFα and a number of other pro-inflammatory cytokines.[42] The direct role of Fas/FasL system in osteoclastogenesis and in mediation of osteoclast apoptosis has now been shown in numerous studies. The interaction of FasL and Fas on osteoclast precursors was shown to increase osteoclastogenesis.[43] In many other studies, the role of Fas/FasL system has been shown to be crucial in mediating apoptosis in osteoclasts and controlling the longevity of osteoclasts,[44,45] whereas other studies have shown that induction of Fas by estrogen is a central protective element against the development of bone loss in female animals.[10,46]

Abnormalities in the immune cell function have long been associated with osteolytic bone conditions such as rheumatoid arthritis. An assessment of both T-cell activation and T regulatory cells in the wild-type and B6.MRL-Fas^{lpr}/J mice was carried out to elucidate the role of T-cell subsets during cartilage resorption and bone remodeling. The findings of this study suggest B6.MRL-Fas^{lpr}/J mice have an active autoimmune state based on the higher percentage of activated T cells and Treg cells in both the spleen and bones at the baseline before fracture. It is interesting to note, however, during the period of active cartilage tissue formation after fracture that the percentage of Treg cells was systemically increased specifically in bone tissues based on their increased numbers within both fractured and unfractured bones. In contrast, the percentage of these cells remained unchanged in the spleen. These findings taken together with the 100- to 200-fold induction of IL-17A suggest that these cells are specifically iTreg cells and that cartilage formation produces factors that promote their formation within bone tissues. This interpretation is further consistent with the decreased or unchanged numbers of activated T cells in callus tissues in the either wild-type or B6.MRL-Fas^{lpr}/J mice, respectively. In this context, these results are similar to the paradoxical findings showing diminished cartilage destruction in a collagen-induced arthritis (CIA) model comparing DBA-lpr/lpr with DBA wild-type mice, even though these mice have a more robust inflammatory state. These authors concluded that the lack of the expected severe disease in DBA-lpr/lpr mice is because of a local attenuating effect of the Fas mutation in pathological processes involving resident joint cells. They further attributed this to alterations in either synovial cells or T-cell populations in the joint and not to the role that Fas plays in mediation of chondrocyte apoptosis.[47] Such findings in conjunction with ours suggest that within cartilage tissues, iTreg cells are protective to cartilage tissue destruction.

Our results also match most of the findings of Nam and colleagues,[48] who examined fracture healing in Rag1-/- mice

that have deficient T- and B-cell function. Although our results showed similar increases in the expression of IL-6, IL-23, and IL-10 in the wild-type mice immediately after fracture, we did not see initial elevation in IL-17F at 3 days after fracture. With the exception of TNFα, our findings showed decreased expression for these pro-inflammatory cytokines in B6.MRL-Fas^{lpr}/J similar to that seen in the Rag1-/- mice. Although these results would appear contradictory in relationship to an active autoimmune state, they would be consistent with the increased percentages of iTreg cells and be suggestive of a compensatory response to the systemic autoimmunity during cartilage tissue formation. In this regard, recent studies by Adamik and colleagues[49] showed that PGE2 and IL-23 plus IL-1β differentially regulate Th17 cytokine expression and synergize to induce IL-17A but not IL-17F, whereas IL-23 plus IL-1β in the absence of PGE2 preferentially induce IL-17F expression. Consistent with these observed combinations of cytokines that differentially regulate the expression of IL-17A and IL-17F are the findings from our prior studies that have shown that both Cox2 expression levels and PGE2 levels in the callus are induced during the period of cartilage tissue formation.[50,51]

It is interesting to note that one of the major complications in SLE patients is osteoporosis.[52] The data from our studies are consistent with human studies that have shown significant trabecular and cortical bone loss,[53] as well as other studies that have shown osteoporotic vertebral fractures in up to 20% of patients with SLE.[54] Other studies have found an association between SLE disease damage and low bone mineral density (BMD) *T*-scores.[55] Although many of these studies are carried out in patients with prolonged SLE, a question of the etiology of the osteoporotic disease is related to the use of glucocorticoids and cyclophosphamide to manage these diseases that by themselves lead to bone loss.[52] In light of the question of the actions of these therapeutics on bone loss independent of the primary actions of SLE, our animal studies would suggest that the systemic SLE pathology itself leads to elevated turnover of bone because our animals do not receive any type of pharmacological treatments during the course of their bone healing. In this regard, our findings, as they relate to the elevated expression of IL-17F at later periods after cartilage resorption when only coupled bone remodeling is taking place, are consistent with a high turnover state of osteoporosis. This is based on recent findings of Nam and colleagues,[48] who showed that IL-17F is highly stimulatory of osteogenesis, as well as other studies that show that it supports osteoclastogenesis by the stimulation of mesenchymal and osteoblast production of RANKL and M-CSF.[56] This conclusion is also consistent with a number of recent studies that have shown that patients who have never received glucocorticoids were observed to have a lower hip bone mineral density than controls, suggesting that SLE per se might induce bone loss.[53] Finally, similar conclusions as ours on the primary actions of the SLE on loss were reached in developmental studies within this same mouse model (B6.MRL-Fas^{lpr}/J) as we are using, which showed that these animals developed low bone mass index phenotype,[57] although the molecular mechanism that led to low bone mass had not been identified in these early studies.

In conclusion, our data show that loss of Fas activity does not effect endochondral bone formation. Although the number of TRAP-positive cells per area of bone and cartilage was greater in the B6.MRL-Fas^{lpr}/J, the rate of cartilage resorption was codependent on chondrocyte apoptosis. During the later periods of coupled remodeling of the primary bone, the B6.MRL-Fas^{lpr}/J fracture calluses are weaker and more porous. This corresponded to a higher ratio of RANKL/OPG at after-fracture days 21 and 28. We determined there were both higher osteoclast activity in the B6.MRL-Fas^{lpr}/J and more osteoblast activity based on more expression of extracellular matrix proteins at later stages in the fracture repair. We conclude from these data that there was a state of high-turnover osteoporosis occurring in the B6.MRL-Fas^{lpr}/J mouse.

Disclosures

All authors state that they have no conflicts of interest.

Acknowledgments

The authors thank Lee Silkman and Zachary Mason for their excellent technical assistance in the postoperative care of mice and in assistance in micro-CT analysis. We acknowledge the assistance of the Flow Cytometry Core Facility at the BU School of Medicine, where the flow cytometry analysis reported in this article was performed. We also thank Dr Amira Hussien for assistance with the statistical analysis.

Research reported in this publication was supported by the National Institute of Arthritis and Musculoskeletal and Skin Diseases of the National Institutes of Health under award no. AR 47045 (LCG) and PO1 AR049920 (TAE). The content is solely the responsibility of the authors and does not necessarily represent the official views of the National Institutes of Health. Institutional support was provided by the Department of Orthopaedic Surgery of Boston University School of Medicine and by Boston University School of Medicine.

Authors' roles: Study design: LCG, DG, ACB, TEA, and EFM. Data collection: MAS, DD, ACB, DC, NAW, and SK. Data analysis: MAS, DC, DG, and ACB. Data interpretation: MAS, ACB, DG, EFM, and LCG. Drafting manuscript: MAS and LCG. Revising manuscript: EFM, ACB, and LCG. Study conduct: LCG and EFM. Approving final version: EFM and LCG.

References

1. Kon T, Cho TJ, Aizawa T, et al. Expression of osteoprotegerin, receptor activator of NF-kappaB ligand (osteoprotegerin ligand) and related proinflammatory cytokines during fracture healing. J Bone Miner Res. 2001;16(6):1004–14.
2. Gerstenfeld LC, Cho TJ, Kon T, et al. Impaired fracture healing in the absence of TNF-alpha signaling: the role of TNF-alpha in endochondral cartilage resorption. J Bone Miner Res. 2003;18(9):1584–92.
3. Lehmann W, Edgar CM, Wang K, et al. Tumor necrosis factor alpha (TNF-alpha) coordinately regulates the expression of specific matrix metalloproteinases (MMPS) and angiogenic factors during fracture healing. Bone. 2005;36(2):300–10.
4. Gerstenfeld LC, Cho TJ, Kon T, et al. Impaired intramembranous bone formation during bone repair in the absence of tumor necrosis factor-alpha signaling. Cells Tissues Organs. 2001;169(3):285–94.
5. Glass GE, Chan JK, Freidin A, Feldmann M, Horwood NJ, Nanchahal J. TNF-alpha promotes fracture repair by augmenting the recruitment and differentiation of muscle-derived stromal cells. Proc Natl Acad Sci USA. 2011;108(4):1585–90.
6. Cho TJ, Lehmann W, Edgar C, et al. Tumor necrosis factor alpha activation of the apoptotic cascade in murine articular chondrocytes is associated with the induction of metalloproteinases and specific pro-resorptive factors. Arthritis Rheum. 2003;48(10):2845.
7. Wallach D, Varfolomeev EE, Malinin NL, Goltsev YV, Kovalenko AV, Boldin MP. Tumor necrosis factor receptor and Fas signaling mechanisms. Annu Rev Immunol. 1999;17:331–3367.

8. Bazzoni F, Beutler B. The tumor necrosis factor ligand and receptor families. N Engl J Med. 1996;334(26):1717–25.
9. Eugster HP, Muller M, LeHir M. Immunodeficiency of tumor necrosis factor and lymphotoxin-alpha double deficient mice. In: Durum S, Muegge K, editors. Cytokine knockouts. Totowa (NJ): Humana Press; p. 103–27. 1998.
10. Nakamura T, Imai Y, Matsumoto T, et al. Estrogen prevents bone loss via estrogen receptor alpha and induction of Fas ligand in osteoclasts. Cell. 2007;130(5):811–23.
11. Wu X, Pan G, McKenna MA, Zayzafoon M, Xiong WC, McDonald JM. RANKL regulates Fas expression and Fas-mediated apoptosis in osteoclasts. J Bone Miner Res. 2005;20(1):107–16.
12. Gibson G. Active role of chondrocyte apoptosis in endochondral ossification. Microsc Res Tech. 1998;43(2):191–204.
13. Roach HI, Erenpreisa J, Aigner T. Osteogenic differentiation of hypertrophic chondrocytes involves asymmetric cell divisions and apoptosis. J Cell Biol. 1995;131(2):483–94.
14. Hashimoto S, Setareh M, Ochs RL, Lotz M. Fas/Fas ligand expression and induction of apoptosis in chondrocytes. Arthritis Rheum. 1997;40(10):1749–55.
15. Aizawa T, Kokubun S, Tanaka Y. Apoptosis and proliferation of growth plate chondrocytes in rabbits. J Bone Joint Surg Br. 1997; 79(3):483–6.
16. Lee FY, Choi YW, Behrens FF, DeFouw DO, Einhorn TA. Programmed removal of chondrocytes during endochondral fracture healing. J Orthop Res. 1998;16(1):144–50.
17. Aizawa T, Kon T, Einhorn TA, Gerstenfeld LC. Induction of apoptosis in chondrocytes by tumor necrosis factor-alpha. J Orthop Res. 2001;19(5):785–96.
18. Chu JL, Drappa J, Parnassa A, Elkon KB. The defect in Fas mRNA expression in MRL/lpr mice is associated with insertion of the retrotransposon. ETn. J Exp Med. 1993;178(2):723–30.
19. Watanabe-Fukunaga R, Brannan CI, Copeland NG, Jenkins NA, Nagata S. Lymphoproliferation disorder in mice explained by defects in Fas antigen that mediates apoptosis. Nature. 1992;356(6367):314–7.
20. Furukawa F, Kanauchi H, Wakita H, et al. Spontaneous autoimmune skin lesions of MRL/n mice: autoimmune disease-prone genetic background in relation to Fas-defect MRL/1pr mice. J Invest Dermatol. 1996;107(1):95–100.
21. Alexander EL, Moyer C, Travlos GS, Roths JB, Murphy ED. Two histopathologic types of inflammatory vascular disease in MRL/Mp autoimmune mice. Model for human vasculitis in connective tissue disease. Arthritis Rheum. 1985;28(10):1146–55.
22. Kelley VE, Roths JB. Interaction of mutant lpr gene with background strain influences renal disease. Clin Immunol Immunopathol. 1985;37(2):220–9.
23. Jepsen KJ, Price C, Silkman LJ, et al. Genetic variation in the patterns of skeletal progenitor cell differentiation and progression during endochondral bone formation affects the rate of fracture healing. J Bone Miner Res. 2008;23(8):1204–16.
24. Morgan EF, Mason ZD, Chien KB, et al. Micro-computed tomography assessment of fracture healing: relationships among callus structure, composition, and mechanical function. Bone. 2009;44(2):335–44.
25. Gerstenfeld LC, Alkhiary YM, Krall EA, et al. Three-dimensional reconstruction of fracture callus morphogenesis. J Histochem Cytochem. 2006;54(11):1215–28.
26. Parfitt AM, Drezner MK, Glorieux FH, et al. Bone histomorphometry: standardization of nomenclature, symbols, and units. Report of the ASBMR Histomorphometry Nomenclature Committee. J Bone Miner Res. 1987;2(6):595–610.
27. Wang K, Vishwanath P, Eichler GS, et al. Analysis of fracture healing by large-scale transcriptional profile identified temporal relationships between metalloproteinase and ADAMTS mRNA expression. Matrix Biol. 2006;25(5):271–81.
28. Cho TJ, Gerstenfeld LC, Einhorn TA. Differential temporal expression of members of the transforming growth factor beta superfamily during murine fracture healing. J Bone Miner Res. 2002;17(3):513–20.
29. Basu R, Hatton RD, Weaver CT. The Th17 family: flexibility follows function. Immunol Rev. 2013;252(1):89–103.
30. Miedlich SU, Zalutskaya A, Zhu ED, Demay MB. Phosphate-induced apoptosis of hypertrophic chondrocytes is associated with a decrease in mitochondrial membrane potential and is dependent upon Erk1/2 phosphorylation. J Biol Chem. 2010;285(24):18270–5.
31. Kim J, Xu M, Xo R, et al. Mitochondrial DNA damage is involved in apoptosis caused by pro-inflammatory cytokines in human OA chondrocytes. Osteoarthritis Cartilage. 2010;18(3):424–32.
32. Ouchi N, Uzuki M, Kamataki A, Miura Y, Sawai T. Cartilage destruction is partly induced by the internal proteolytic enzymes and apoptotic phenomenon of chondrocytes in relapsing polychondritis. J Rheumatol. 2011;38(4):730–7.
33. Park D, Spencer JA, Koh BI, et al. Endogenous bone marrow MSCs are dynamic, fate-restricted participants in bone maintenance and regeneration. Cell Stem Cell. 2012;10(3):259–72.
34. Iqbal J. Does TNF have anti-osteoclastogenic actions? Ann NY Acad Sci. 2006;1068:234–9.
35. Kaplan DL, Eielson CM, Horowitz MC, Insogna KL, Weir EC. Tumor necrosis factor-alpha induces transcription of the colony-stimulating factor-1 gene in murine osteoblasts. J Cell Physiol. 1996;168(1):199–208.
36. Cenci S, Weitzmann MN, Roggia C, et al. Estrogen deficiency induces bone loss by enhancing T-cell production of TNF-alpha. J Clin Invest. 2000;106(10):1229–37.
37. Zhang YH, Heulsmann A, Tondravi MM, Mukherjee A, Abu-Amer Y. Tumor necrosis factor-alpha (TNF) stimulates RANKL-induced osteoclastogenesis via coupling of TNF type 1 receptor and RANK signaling pathways. J Biol Chem. 2001;276(1):563–8.
38. Yao Z, Li P, Zhang Q, et al. Tumor necrosis factor-alpha increases circulating osteoclast precursor numbers by promoting their proliferation and differentiation in the bone marrow through up-regulation of c-Fms expression. J Biol Chem. 2006;281(17):11846–55.
39. Lam J, Takeshita S, Barker JE, Kanagawa O, Ross FP, Teitelbaum SL. TNF-alpha induces osteoclastogenesis by direct stimulation of macrophages exposed to permissive levels of RANK ligand. J Clin Invest. 2000;106(12):1481–8.
40. Li P, Schwarz EM, O'Keefe RJ, et al. Systemic tumor necrosis factor alpha mediates an increase in peripheral CD11b high osteoclast precursors in tumor necrosis factor alpha-transgenic mice. Arthritis Rheum. 2004;50(1):265–76.
41. Cullen CM, Bonventre PF, Heeg H, Bluethmann H, Mountz JD, Edwards CK 3rd. A fas antigen receptor mutation allows development of toxic shock syndrome toxin-1-induced lethal shock in V beta 8.2 T-cell receptor transgenic mice. Pathobiology. 1995; 63(6):293–304.
42. Anam K, Amare M, Naik S, Szabo KA, Davis TA. Severe tissue trauma triggers the autoimmune state systemic lupus erythematosus in the MRL/++ lupus-prone mouse. Lupus. 2009;18(4):318–31.
43. Park H, Jung YK, Park OJ, Lee YJ, Choi JY, Choi Y. Interaction of Fas ligand and Fas expressed on osteoclast precursors increases osteoclastogenesis. J Immunol. 2005;175(11):7193–201.
44. Roux S, Lambert-Comeau P, Saint-Pierre C, Lepine M, Sawan B, Parent JL. Death receptors, Fas and TRAIL receptors are involved in human osteoclast apoptosis. Biochem Biophys Res Commun. 2005;333(1): 42–50.
45. Imai Y, Youn MY, Kondoh S, et al. Estrogens maintain bone mass by regulating expression of genes controlling function and life span in mature osteoclasts. Ann NY Acad Sci. 2009;1173(Suppl 1):E31–9.
46. Krum SA, Miranda-Carboni GA, Hauschka PV, Carroll JS, Lane TF, Freedman LP, Brown M. Estrogen protects bone by inducing Fas ligand in osteoblasts to regulate osteoclast survival. EMBO J. 2008; 6;27(3):535–45.
47. Hoang Tu-Rapp H, Hammermüller A, Mix E, et al. Aproinflammatory role for Fas in joints of mice with collagen-induced arthritis. Arthritis Res Ther. 2004;6(5):R404–14.
48. Nam D, Mau E, Wang Y, et al. T-lymphocytes enable osteoblast maturation via IL-17F during the early phase of fracture repair. PLoS One. 2012;7(6):e40044.
49. Adamik J, Henkel M, Ray A, Auron PE, Duerr R, Barrie A. The IL17A and IL17F loci have divergent histone modifications and are differentially regulated by prostaglandin E2 in Th17 cells. Cytokine. 2013;64(1): 404–12.

50. Gerstenfeld LC, Thiede M, Seibert K, et al. Differential inhibition of fracture healing by non-selective and cyclooxygenase-2 selective non-steroidal anti-inflammatory drugs. J Orthop Res. 2003;21(4): 670–5.
51. Gerstenfeld LC, Al-Ghawas M, Alkhiary YM, et al. Selective and nonselective cyclooxygenase-2 inhibitors and experimental fracture-healing. Reversibility of effects after short-term treatment J Bone Joint Surg Am. 2007;89(1):114–25.
52. Lane NE. Therapy insight: osteoporosis and osteonecrosis in systemic lupus erythematosus. Nat Clin Pract Rheumatol. 2006;2(10):562–9.
53. Houssiau FA, Lefebvre C, Depresseux G, et al. Trabecular and cortical bone loss in systemic lupus erythematosus. Br J Rheumatol. 1996; 35(3):244–7.
54. Bultink IE, Lems WF, Kostense PJ, Dijkmans BA, Voskuyl AE. Prevalence of and risk factors for low bone mineral density and vertebral fractures in patients with systemic lupus erythematosus. Arthritis Rheum. 2005;52(7):2044–50.
55. Lee C, Almagor O, Dunlop DD, et al. Disease damage and low bone mineral density: an analysis of women with systemic lupus erythematosus ever and never receiving corticosteroids. Rheumatology (Oxford). 2006;45(1):53–60.
56. Lee Y. The role of interleukin-17 in bone metabolism and inflammatory skeletal diseases. BMB Rep. 2013;46(10):479–83.
57. Wu X, McKenna MA, Feng X, Nagy TR, McDonald JM. Osteoclast apoptosis: the role of Fas in vivo and in vitro. Endocrinology. 2003;144(12):5545–55.